ADVANCED SUSTAINABLE SYSTEMS
www.advsustainsys.com

Natural Jute Fibre-Based Supercapacitors and Sensors for Eco-Friendly Energy Autonomous Systems

*Libu Manjakkal, Fabiane Fantinelli Franco, Abhilash Pullanchiyodan, Mario González-Jiménez, and Ravinder Dahiya**

Environmentally friendly energy devices and systems are of increasing interest for the circular economy and sustainable information and communications technology. To this end, an energy-autonomous system comprised of natural jute fiber-based supercapacitor (SC) and sensors (temperature and humidity) is presented. This material is coated with poly(3,4-ethylenedioxythiophene) polystyrene sulfonate (PEDOT:PSS)/single-walled carbon nanotubes as the electrode and cellulose-based material as a separator. Further, a newly prepared hydroxyethyl cellulose-potassium chloride based gel is used as the electrolyte. The observed capacitance is nearly twice the value reported for similar SCs. The energy and power densities of the presented SC are 0.712 μWh cm^{-1} and 3.85 μW cm^{-1}, respectively at a capacitance of 8.65 mF cm^{-1} and an applied current of 0.1 mA. The fabricated temperature sensor shows a relative change in response of 0.23% °C^{-1} from 24 to 35 °C and the humidity sensor exhibits a sensitivity of 1.5 Ω/%RH (relative change of 0.20%) up to 50%RH. Developed using sustainable and biocompatible materials, the presented SC can power the jute-fiber based sensors, thus demonstrating an attractive eco-friendly solution for applications such as wearables, grain sacks, and bags.

1. Introduction

The need to power portable electronic systems for ever-expanding wearables, connected objects, information and communications technology (ICT) devices, electric vehicles, etc., has led to a significant rise in the use of conventional energy storage devices such as Li-ion batteries.[1–3] Such devices offer high energy density and reliable power output, but often they are developed with environmentally unfriendly materials (e.g., acidic electrolytes in Li batteries) and add to the issue of electronic waste.[1,4] As a result, it is increasingly becoming critical to develop eco-friendly devices, using materials that are sustainable and can be reused or naturally discarded. In this regard, the natural fibers (e.g., natural fibers with conductive nanoparticles composites) have been engineered in recent years to develop conductive electrodes[5,6] or energy devices such as batteries and supercapacitors (SC).[7] Similarly, non-toxic or biocompatible electrolytes such as sweat or sweat equivalents have also been explored[8] for sustainable energy storage.[9,10] Such devices make an excellent beginning for the long journey toward the development of electronics that complies with the ethos of circular economy and will revolutionize emerging applications such as wearables, smart packages, robotics, and electric vehicles.[3,11,12]

Herein we present an eco-friendly energy autonomous system comprising of natural jute fiber-based temperature and humidity sensors which are powered by a SC–also based on jute-fiber. The SC uses poly(3,4-ethylenedioxythiophene) polystyrene sulfonate (PEDOT:PSS) coated jute fiber functionalized with single-walled carbon nanotube (SWCNT) as the electrode and a new hydroxyethyl cellulose (HEC) with KCl salt-based gel electrolyte. A key characteristic of the sustainable energy systems is that they use environmentally friendly and/or abundantly available materials as substrates, current collector, active electrode, separator, and electrolytes. In this regard, our jute-fiber-based approach is an attractive route as it is eco-friendly, biodegradable, and recyclable.[6,13] For example, it can be recycled and reused to obtain a carbon electrode for the fabrication of the SC.[14] As the second most-produced natural fiber in the world (after cotton), jute is a readily available low-cost material. It comprises of cellulose (70 wt%), hemicellulose (15 wt%), and lignin (10 wt%).[15] The hydroxyl groups, the main functional groups in cellulose, are involved in a number of intra- and intermolecular hydrogen bonds, leading to the formation of ordered crystalline arrangements aligned along the fiber length. The high tensile and flexural strength resulting from this arrangement makes jute fibers an attractive substrate for flexible devices such as SCs. Further, their ability to be woven into different forms and shapes[16,17] make them suitable for application such as wearables. Given these properties, it

Dr. L. Manjakkal, F. F. Franco, Dr. A. Pullanchiyodan, Prof. R. Dahiya
Bendable Electronics and Sensing Technologies (BEST) Group
James Watt School of Engineering
University of Glasgow
Glasgow G12 8QQ, UK
E-mail: Ravinder.Dahiya@glasgow.ac.uk
Dr. M. González-Jiménez
Chemical Photonics Group
Department of Chemistry
University of Glasgow
Glasgow G12 8QQ, UK
The ORCID identification number(s) for the author(s) of this article can be found under https://doi.org/10.1002/adsu.202000286.

DOI: 10.1002/adsu.202000286

surprising that jute fiber has been largely ignored when it comes to fibers-based devices.

The jute fibers need to be functionalized with conductive materials (e.g., Ag nanoparticle and carbon nanotubes)[17,18] to develop sustainable electrodes. This is because the cellulose and lignin present in the jute fibers act as insulators. Currently, most of the fiber- or textile-based SCs use metal coated cloth, which suffers from issues such as chemical instability due to reaction with electrolytes.[19] On the contrary, due to high cellulose content (≈70%), the jute fiber could absorb aqueous active electrode inks including those based on organic conductive polymer and aqueous nanoparticle carbon[8,20]–thus leading to SCs with improved performance. The choice of electrolytes and their wettability for longer periods also governs the high performance of energy devices such as SCs. Herein, we have used a newly prepared HEC-KCl based gel as the electrolyte to overcome the traditional issue of crystallization of the metal salt. Neutral gel electrolytes such as polyvinyl alcohol (PVA)[10] crystallize or salt out (like KCl, sodium chloride (NaCl), and sodium sulfate (Na_2SO_4)) easily during the electrolyte preparation.[21] The HEC-KCl based gel electrolyte used here is biocompatible and this is an attractive feature for applications such as wearables where health hazard due to leakage of the electrolyte can be a major concern. Further, the film-forming capability and high gluiness of HEC can enhance the electrolyte – electrode bonding, allowing the SC to exhibit stable capacitive behavior against mechanical deformation such as bending.[22] Further, it can promote ion diffusion from the bulk electrolyte and hence improve the SC performance.[20] The HEC electrolyte applied here on the cellulose-based separators allowed for a longer lasting electrode wettability (one of our tests shows more than 13 days (5000 cycles) of continuous charging-discharging measurement).

In this work, the materials used for the fabrication of the SC and the sensors are biocompatible and cause less pollution when compared to traditional energy storage devices. Further by using natural fibers for electronics and energy storage application, this work proposes new application for natural fibers. With a focus on the sustainable materials-based energy storage devices and energy-autonomous systems, this work supports the united nations sustainable development goals such as i) sustainable cities and communities, ii) affordable and clean energy, and iii) responsible consumption and production.

2. Results and Discussion

2.1. Design of the SC

In this work, PEDOT: PSS coated jute fiber is used for the fabrication of SC due to better stability, uniform film property, excellent conductivity, and higher electroactivity in comparison with other conducting polymers.[23] The high cellulose content (≈70%) of the jute fiber allows them to absorb the polymer ink in the bulk. However, an electrode redox reaction in the PEDOT: PSS could lead to the degradation of the polymer coating. We also observed that PEDOT: PSS has low intercalation capacitance when reacting with the electrolyte. To overcome this, we functionalized PEDOT: PSS with SWCNT on top, as it offers high electrical conductivity, high aspect ratio, large surface area, and excellent electrochemical activity and chemical stability.[24] Further, it enhances the conductivity of the electrode as the SWCNT network provides multiple pathways for electron and ion transportation. It was found that the electrochemical double-layer capacitance (EDLC) from SWCNT and the pseudocapacitance along with EDLC from PEDOT: PSS results in excellent electrochemical performance of the SC. The schematic of the SC is shown in **Figure 1**a with a cross-section of the electrode (Figure1b) and an image of the fabricated SC is in Figure 1c. The positive (K^+) and negative (Cl^-) ions from HEC-KCl electrolyte are distributed in the electrode (Figure 1d). Depending on the polarity of the electrode during charging, an electrochemical double layer (edl) is formed on the surface of each fiber electrode as shown in Figure 1e.

2.2. Structural Analysis

Fourier transform infrared spectroscopic analysis shows the presence of functional groups from jute fiber (**Figure 2**1), cellulose/polyester cloth (Figure 2a), jute with PEDOT: PSS (Figure 2b), jute with PEDOT: PSS/SWCNT (Figure 2b) and HEC-KCl gel electrolyte (Figure 2c). The spectra of jute and cloth (Figure 2a) share characteristic bands of moieties of polysaccharides. i) The band associated with sugar alcohols between 3600 and 3000 cm^{-1}, with a small characteristic peak of O—H stretching in cellulose at ≈3330 cm^{-1}. ii) A weaker band associated with the stretching of C—H bonds can be seen between 3000–2800 cm^{-1}. This vibration justifies the band that appears in the region between 1400 and 1300 cm^{-1}. iii) The intense peak between 1165 and 900 cm^{-1} is mainly due to the combination of two peaks of absorption by the C—O bonds. Between 1165 and 1110 cm^{-1} the stretching vibrations of C—O—C bonds in ethers can be observed. Likewise, between 1070 and 950 cm^{-1} the stretching of C—O bonds alcohols is present. Cellulose is rich in both functional groups. iv) The peak that appears in at lowest wavenumber region (< 730 cm^{-1}) of our spectra is due to the bending vibration of the C—H bonds. The jute spectrum also shows peaks associated with its higher proportion of lignin, rich in phenyl groups. This justifies the small peaks between 1700 and 1450 cm^{-1} associated with the C—C stretching in the aromatic ring. For jute fiber treated with PEDOT: PSS, the spectrum (Figure 2b) shows $-CH_2$ bonding with the two twin peaks at 2920 and 2860 cm^{-1}. The two characteristic peaks at 1463 and 797 cm^{-1} show the presence of thiophene in the polymer mixture. The broad band between 3600 and 3000 cm^{-1} is due to the stretching vibrations of C—H bonds. The optical properties of the PEDOT: PSS coated jute fiber functionalized with SWCNTs (Figure 2b) show a combination of broad absorption of infrared radiation. The reflection of the higher wavenumber part of the light makes it difficult to measure the infrared spectrum. Even so, from the above spectrum, the absorption of SWCNTs can be discerned. Finally, the HEC–KCl gel electrolyte spectrum was obtained by placing a small sample on a glass microscope slide (Figure 2c). Due to the strong absorption of this material, we could not measure below 2000 cm^{-1}. In addition, because of the irregular surface of HEC after drying, the absorption on the other side of the spectrum is also distorted. However, the stretching vibration bands of the O—H and C—H bonds (3600–3000 cm^{-1} and 3000–2800 cm^{-1}, respectively) are perfectly visible.[25]

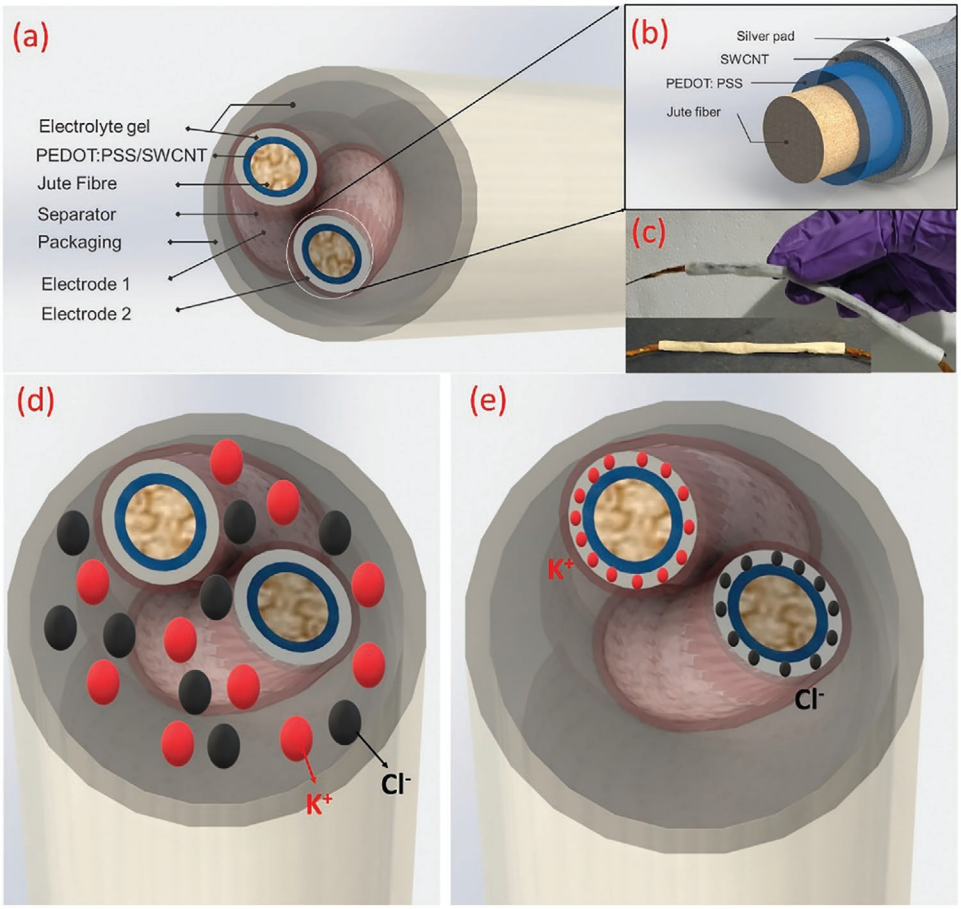

Figure 1. a) Schematic representation of the jute fiber-based SC. b) The cross-section of the electrode, c) image of the fabricated SC, d) Positive (K^+) and negative (Cl^-) ions distributed in the SC electrodes, and e) ions distribution during charging of the electrodes.

2.3. Electrochemical Performances of the Devices

The electrochemical impedance spectroscopic (EIS) analysis, through the Nyquist plots (**Figure 3**a), confirms faster ion transport of PEDOT: PSS/SWCNT electrode as compared to PEDOT: PSS electrode by offering low impedance (as shown in Bode impedance plot in Figure 3b). The equivalent circuit of SCs (inset of Figure 3b) could predict the electrical properties, which are summarized in **Table 1**. The equivalent fitting shows that on the application of a potential the ions from the electrolyte (K^+ and Cl^-) interact with the surface of the film and an edl gets generated through non-Faradaic reaction, eventually leading to a double-layer capacitance (C_{dl}) formation. The analyzed results (Table 1) show that the PEDOT: PSS/SWCNT based SC shows

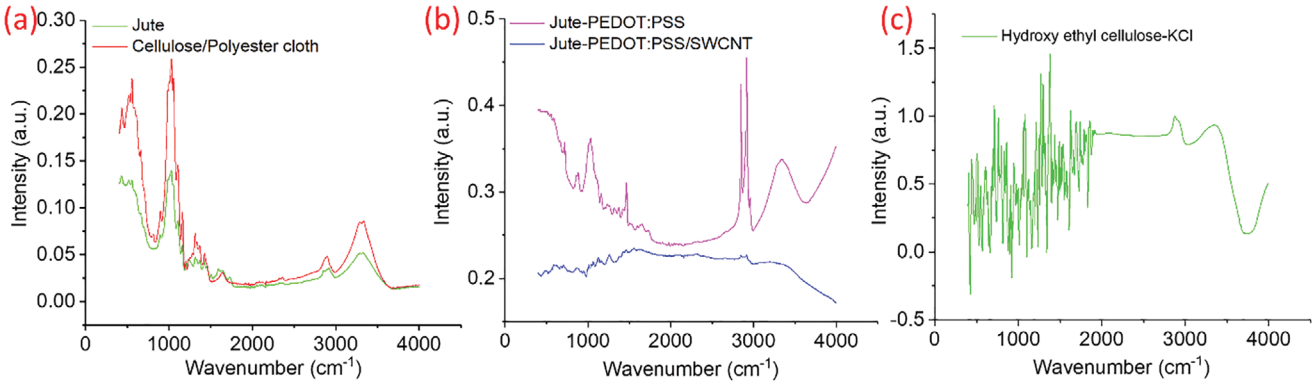

Figure 2. Infrared spectrum of a) jute and bare Cellulose/Polyester based cloth, b) jute–PEDOT PSS and Jute–PEDOT PSS + SWCNT c) HEC–KCl based gel electrolyte.

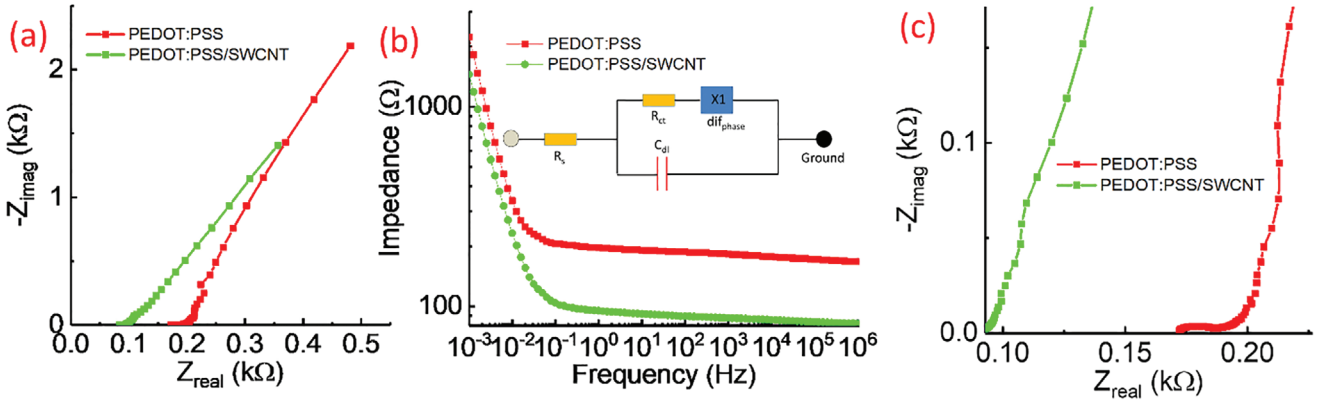

Figure 3. a,b) Comparison of Nyquist and Bode impedance plots for PEDOT: PSS and PEDOT: PSS/SWCNT based SCs (inset shows equivalent circuit). c) Nyquist plot at a high-frequency range.

more than three times higher C_{dl} value as compared to the PEDOT: PSS based SC. It was noted that the π–π interaction between the thiophene rings of PEDOT and the SWCNTs helps to delocalize the electrons in the PEDOT:PSS chain, which in turn increases the conductivity of the film.[26] The SWCNT coated on the top of PEDOT: PSS matrix further enhances the conductivity of the electrode by providing multiple pathways for electron and ion transport with excellent chemical stability.[24] The enhanced conductivity leads to better electrode–ion interaction as evident from the lower solution resistance (R_s) of PEDOT: PSS/SWCNT based SCs (88 Ω) in comparison with the one based on PEDOT: PSS (147 Ω).

Surface roughness also plays an important role, particularly in determining the resistance of electrode–electrolyte contacts. To this end, we measured the roughness of the film-coated on the top of jute fiber through the scanning electron microscopic (SEM) images, as shown in Figure S1, Supporting Information. Comparing with the C_{dl}, we noted that the magnitude of the diffusion capacitance (C_d) is higher (it is in the mF range). The diffusion capacitance occurs in the bulk phase of the active materials due to the redox-dependent insertion of the ions from the electrolyte. It was noted that the ions from the electrolyte diffuse into the pores of the PEDOT: PSS electrode and contribute to the pseudocapacitance due to a redox reaction of the conjugated polymer. Here due to the presence of SWCNT, the diffusion resistance (R_d) and the charge transfer resistance (R_{ct}) have lower values. At high frequencies (Figure 3c), a minor R_{ct} (1.8 mΩ) with an invisible semicircle was found for the PEDOT: PSS/SWCNT electrode, while the PEDOT: PSS electrode showed a larger value of ≈34.Ω, obtained from the diameter of the semicircle at the high frequency. Hence, due to the low ionic diffusion resistance the PEDOT: PSS/SWCNT electrode-based SC shows a high pseudocapacitance. Through EIS analysis, it was found that the PEDOT: PSS/SWCNT electrode-based SC exhibited higher intercalation capacitance[12] (113 mF at 1 mHz) as compared to the PEDOT: PSS electrode (72 mF at 1 mHz). This is confirmed by the low impedance in Bode plots, shown in Figure 3b. Thus, significant enhancement in the electron/ion transport is achieved with the PEDOT: PSS/SWCNT electrode.

Table 1. The variation of parameters for the PEDOT: PSS and PEDOT: PSS/SWCNT based SCs obtained from equivalent fitting of the Nyquist plots.

Parameters	PEDOT: PSS	PEDOT: PSS/SWCNT
R_s (Ω)	147.18	85.88
R_{ct} (Ω)	34.3	0.0018
C_{dl} (F)	6.03e-9	2.53e-6
R_d (Ω)	92.8	79.93
C_d (F)	0.0065	0.0093

The cyclic voltammetry (CV) curves (at a scan rate of 10 mV s^{-1} in **Figure 4**a and 1 mV s^{-1} in Figure 4b) of the PEDOT: PSS and PEDOT: PSS/SWCNT based SCs exhibited a pseudo rectangular shape at scan rates of 1–10 mV s^{-1} (shown in Figure 4c for PEDOT: PSS/SWCNT electrode). The CV curves indicated good capacitive behavior of the fabricated SCs. Distorted rectangular curves found for both SCs, in the case of high scan rate (50 and 100 mV s^{-1}), could be attributed to a limited diffusion rate constant.[24] The specific capacitance (C_{sp}) of SCs were obtained by using the expression given in the supporting information. The trends of the C_{sp} at varying scanning rates for the PEDOT: PSS and PEDOT: PSS/SWCNT SCs are shown in Figure 4d. It was found that the PEDOT: PSS/SWCNT on jute fiber shows higher C_{sp} (17 mF cm^{-1}) as compared to the PEDOT: PSS coated on jute (14 mF cm^{-1}) at a scan rate of 1 mV s^{-1}. This is due to the influence of edl formation (Figure 1c) and redox reaction in conducting polymers, as confirmed by the EIS analysis. The observed value of the capacitance is higher than or at least comparable with the reported fiber-based SCs fabricated using carbon, metal oxides, and polymer materials[27,28] (shown in Table S1, Supporting Information).

The galvanostatic charging–discharging (GCD) analysis (Figure 4e) shows an approximately linear relationship between charging and discharging voltage with time. The comparison of GCD plots for the PEDOT: PSS and PEDOT: PSS/SWCNT based SCs in Figure 4e shows that both SCs have fast charging/discharging capability and exhibit good capacitive properties. Compared to the stable linear response of PEDOT: PSS/SWCNT, a variation of linearity in the charging–discharging curve is observed for the PEDOT: PSS electrode. This could

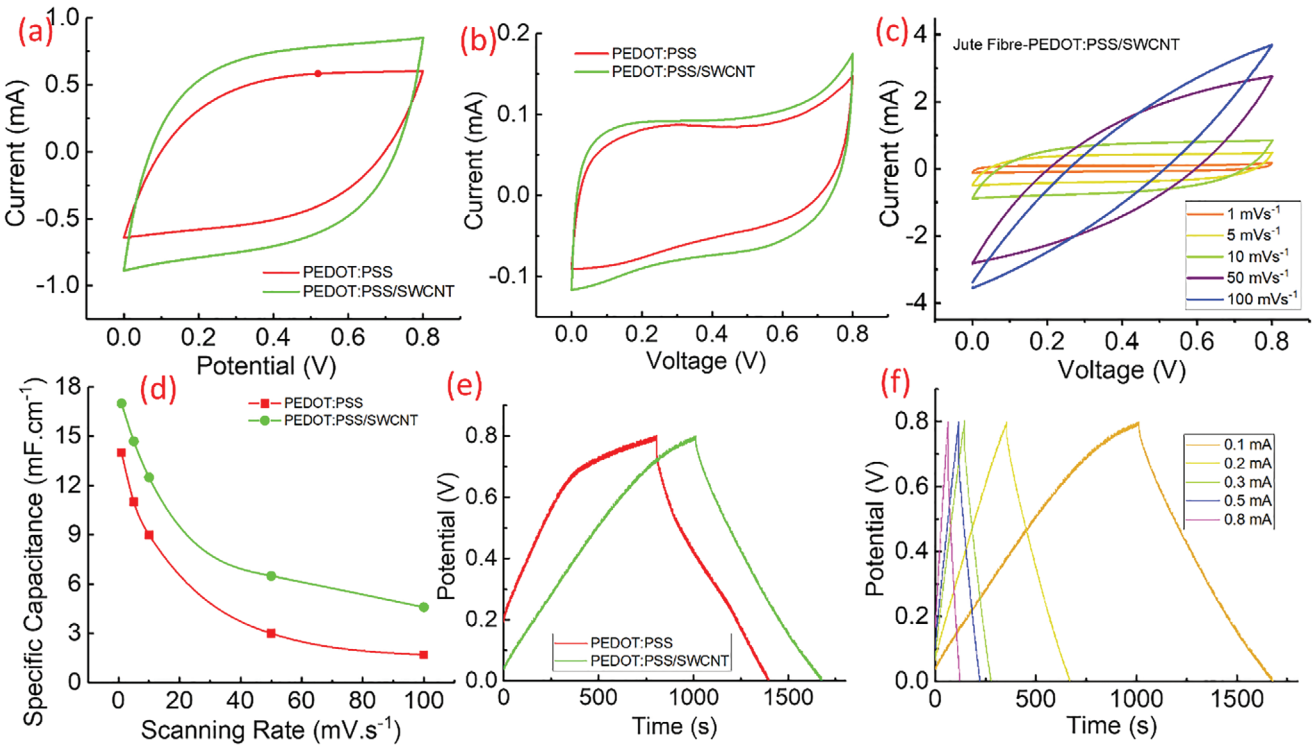

Figure 4. a,b) Comparison of CV plot for PEDOT:PSS and PEDOT:PSS/SWCNT based SCs at 10 and 1 mV s^{-1}, respectively, c) CV spectra at different scanning rate, d) measured specific capacitance of the SCs, e) GGCD plot for the PEDOT:PSS and PEDOT:PSS/SWCNT based SCs, f) GCD plot for PEDOT:PSS/SWCNT at different applied current densities.

be due to redox reactions occurring in the uncoated PEDOT: PSS. The GCD curves at different applied currents were also measured for the two types of SCs (Figure 4f). The measured C_{sp}, after considering the IR_{drop}, shows a slightly higher value (8.65 mF cm^{-1}) for the PEDOT: PSS/SWCNT SC when compared to the PEDOT: PSS SC (8 mF cm^{-1}), at an applied current of 0.1 mA. For the same C_{sp}, the energy and power densities of the PEDOT: PSS/SWCNT SC are 0.712 μWh cm^{-1} and 3.85 μW cm^{-1}, respectively. These values are slightly higher than those observed for the PEDOT: PSS electrode (0.608 μWh cm^{-1} and 3.69 μW cm^{-1}). The observed energy density for the developed SC is higher than or comparable with the reported carbon or metal fiber-based SCs (e.g., 0.70 μWh cm^{-1} and 13.7 μW cm^{-1} carbon micro-fibers coated with SWCNTs;[27] 1.089 μWh cm^{-1} for MnO_2 coated carbon fibers;[29] 0.085 μWh cm^{-1} in carbon nanotube/ordered mesoporous carbon composite fibers based SC[30]).

The performance of PEDOT: PSS/SWCNT on jute fiber was evaluated for 5000 charging–discharging cycles at 0.3 mA charging current. We observed that the SC took almost 13 days to complete this cyclic measurement. The data for initial and final cycles were stored and plotted in **Figure 5**a,b along with the observed drift in voltage. The study shows the stability of the SC for long charging–discharging measurements when HEC based electrolytes are used. The measured capacitive retention is 60% (after considering the potential drift of 0.22 V). If we do not consider the potential drift (i.e., keeping 0.8 V as constant) the capacitive retention is 52%. To evaluate the suitability of the presented SC for practical applications, its performance was also tested for static bending (Figure S2a, Supporting Information, shows the experimental setup) and negligible variation in electrical properties was observed (Figure S2b, Supporting Information). Further, the variation of electrical properties (resistance and capacitance) at the AC signal of 1 kHz under dynamic cyclic bending was evaluated as shown in Figure 5c. The cyclic bending test shows no significant change in the performance (capacitance variation is ± 0.02 mF) of the SC before and after 300 bending cycles (Figure 5c,d). The PEDOT: PSS–jute fiber SC was also placed in a beaker (without any packaging) and the electrochemical properties (discussed in Figure S3, Supporting Information, by using PVA–KCl gel electrolyte) showed excellent performance. The energy and power densities of this SC show that it could be potentially used for low power sensors that require voltage less than 500 mV and μA current range for their operation. To demonstrate this possibility, we also developed two jute fiber-based sensors as described below.

2.4. Design of the Jute Fiber-Based Sensors

The push toward more environmentally sustainable is also driving the development of sensors on cellulose-based materials with biocompatible or biodegradable electrodes. This is also needed to overcome the traditional issues with standard electrodes such as the hazardous nature of the employed materials. The jute fiber-based sensors are attractive in this context. They could be potentially employed to monitor the quality of food,

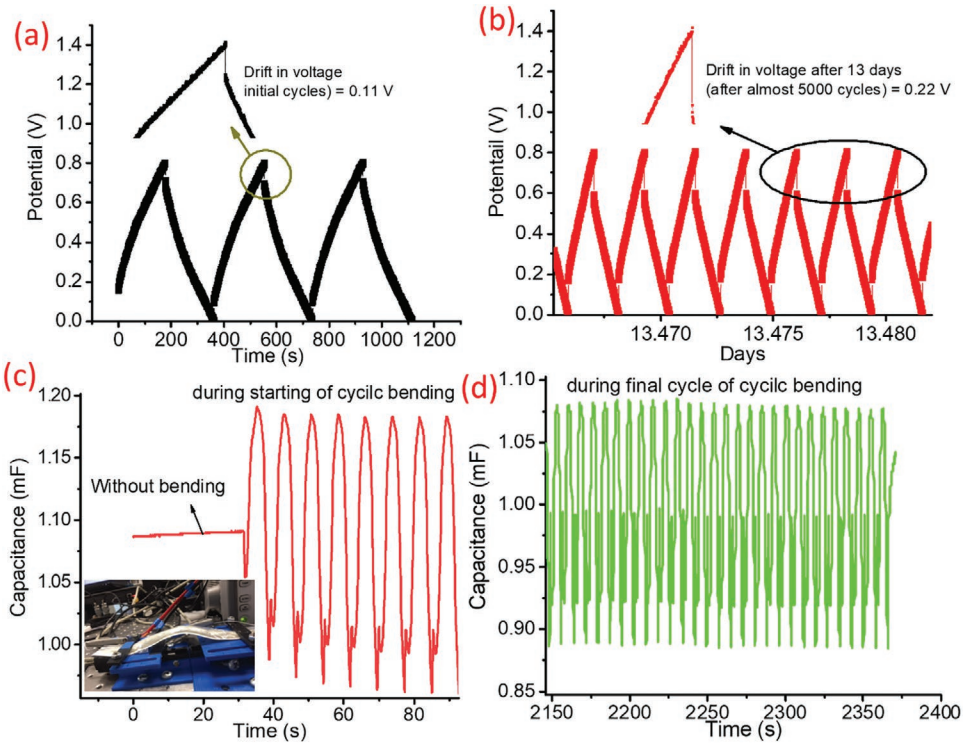

Figure 5. a,b) Initial and final cycles of long charging–discharging (5000 cycles) analysis along with the potential drift. The performances of the jute-fibre based SCs under dynamic bending conditions c) without bending and initial cycles, d) during final cyclic bending.

environment, and health. Here, we designed the electrodes by drop-casting the PEDOT: PSS ink on jute fiber, similar to the SC electrode fabrication (as shown in **Figure 6**a) (PEDOT: PSS ink was prepared by mixing with ethylene glycol (EG)). Using this electrode, humidity and temperature sensors were fabricated. For the temperature sensor, the electrode was covered

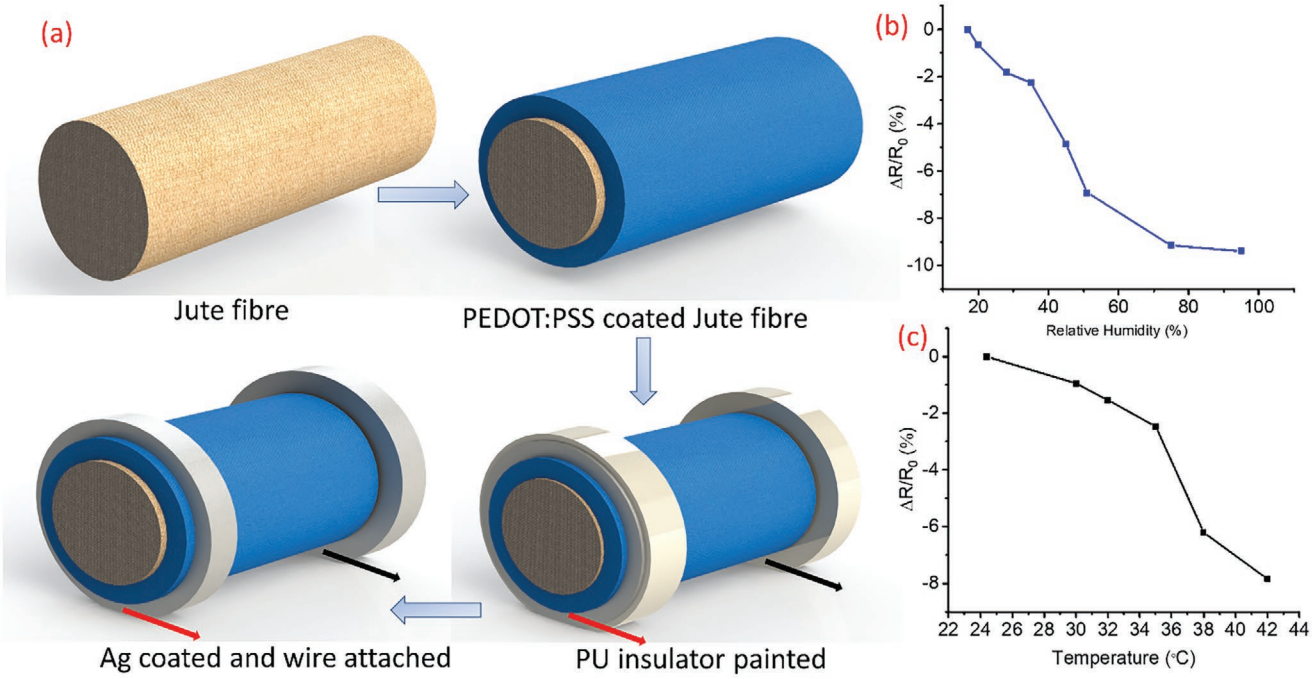

Figure 6. a) Fabrication steps of the jute fibre/PEDOT: PSS electrode for temperature and humidity sensing. b,c) Performances of humidity and temperature sensors, respectively.

with cling film to avoid the influence of humidity on the surface of the electrode.

2.5. Performance of Jute Fiber-Based Sensors

The PEDOT: PSS coated jute-fiber based humidity sensor shows an almost linear relationship between the relative humidity (RH) and resistance up to nearly 50% RH, with resistance decreasing with increasing humidity (slope of 1.5 Ω/%RH or 0.20%/RH with a linear coefficient of 0.9552). The response steadily reaches a plateau from 50 to 95% RH. With increasing RH, a decrease in resistance was observed (shown in Figure 6b) as the water molecules are adsorbed on the surface of the PEDOT: PSS film and an electrostatic field is caused by the hydronium ion (an edl formation) – which promotes higher ionic conduction.[31] Considering the significant dipole moment of water molecules, their adsorption on the surface of the PEDOT: PSS may increase the charge carrier density of the film, as the doping materials influence the overall conductivity of semiconducting layers.[32] Furthermore, the water layer could dissolve some of the PSS protons, changing the hole conductivity of PEDOT: PSS to an ionic conductivity.[33] Recent studies, showing the swelling behavior of PEDOT:PSS in high humidity environments, have noted water uptake could be reduced by post-treating of PEDOT:PSS layer with EG.[34] The treatment with EG could reduce the PSS content inside the film, increasing the film hydrophobicity.[34] This could explain why the resistance variation is lower at higher humidity values.

For temperature evaluation, the PEDOT: PSS coated jute fiber was inserted in water (after packing the electrode). The measurement in water gives a uniform distribution of the temperature around the circular fiber electrode. We noted that with increasing temperature the resistance of the electrode decreased (shown in Figure 6c) and it depends on the length of the electrode (here the active length of the electrode is 2 cm). The decrease in the resistance of the PEDOT: PSS based sensor is attributed to the shift in the thermal energy which leads to microstructural changes in PEDOT: PSS as previously discussed.[35,36] The sensor shows an almost linear decrease in the resistance (from 24 to 35 °C with a slope of 0.23% $°C^{-1}$) with a linear coefficient of 0.9701) and exponential decrease at high temperatures. Here the active electrode (PEDOT: PSS) is a p-type semiconductor in which increasing temperature causes excitation of the electrons from the conduction band (CB) to the valence band (VB).[36–38] This thermal energy creates a hole in the VB and the material shows a negative temperature coefficient of the resistance characteristics. The magnitude of the resistance variation could be varied by changing the conductivity of PEDOT: PSS, for example, by varying the EG concentration and the dimension of the electrode.[36,37] Stable performance of these conductive fiber-based sensors for real-time applications could be obtained by applying constant power. For this, a demo was developed as discussed below.

2.6. Energy Autonomous System

The development of devices alone is insufficient when it comes to bringing a positive change in terms of sustainable ICT for various applications. There is a need to focus on the energy autonomy of a full system. In this regard, we demonstrate the jute fiber-based sensors and SC integrated on a jute bag along with a flexible solar cell. The energy generated by the flexible solar cells is stored in the jute fiber SC (shown in **Figure 7**a), which is then used to operate the sensors. The charging and

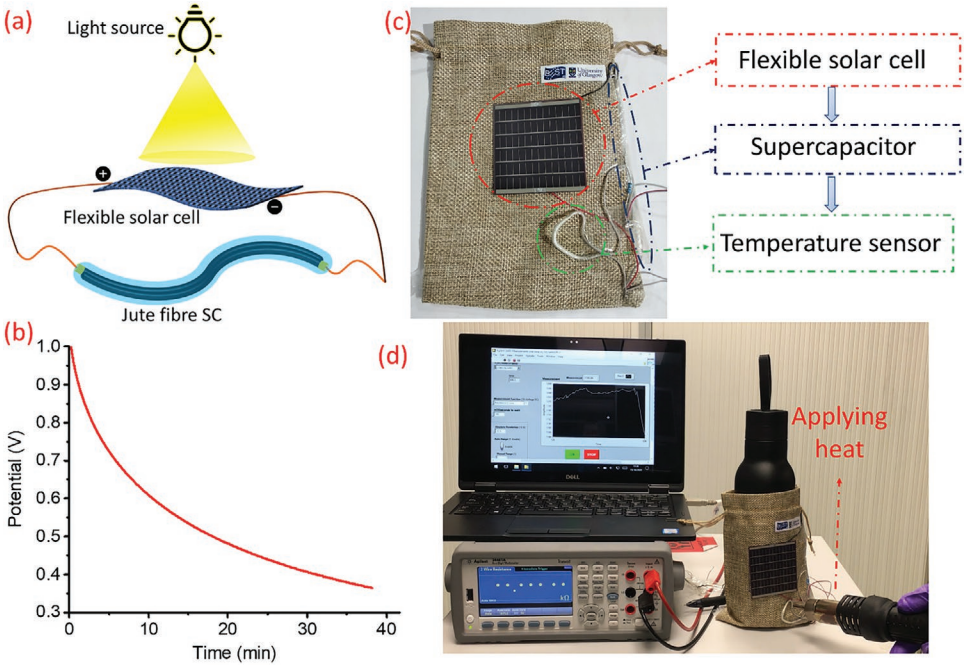

Figure 7. a) Schematic for SC charging using a flexible solar cell. b) Self-discharging of the SC integrated on c) the jute bag along with solar cell and temperature sensor. d) The response of SC powered temperature sensor.

discharging of the SC (PEDOT: PSS/SWCNT) by using the solar cell is shown in Figure S4, Supporting Information. Initially, the SC was fully discharged and again charged using solar cell (up to 1 V). The self-discharging of SC was observed using the multimeter. The results show the discharge from 1 to 0.7 V in 348 s. However, at the lower voltage, the self-discharging time was much longer (e.g., from 0.7 to 0.4 V it took more than 25 min), as shown in Figure 7b. These results are useful as the operating voltage of sensors in many practical applications range between 100 to 500 mV (depending on the type of materials used for fabrication) and in this regard our SC is attractive. As proof of concept the flexible solar cell, attached to the jute bag, was used to charge the SC (shown in Figure 7c). Once the SC is charged, the temperature sensor on the bag is powered as shown in Figure 7d (block diagram for powering the temperature sensor is given in Figure S5, Supporting Information). When hot air was blown on the jute-based temperature sensor, the resistance of the electrode decreased over time (with response time less than 1 min) in line with the performance discussed above. The sensor returned to its original stage when the source of heat was removed. A real-time demo is shown in Movie S1, Supporting Information. Such energy-autonomous-sensitized bags could provide rich information about the content inside (e.g., food, grain, and other items). As an example, the jute based smart-sacks with moisture, temperature, and CO_2 sensors could provide critical information needed to minimize post-harvest losses of grains.

3. Conclusions

In summary, this paper demonstrated a modified jute-fiber based PEDOT: PSS/SWCNT electrode and cellulose as a major component and their use for development of energy-autonomous system having temperature and humidity sensors and SC. To this end, we also prepared a new HEC–KCl based gel electrolyte. The PEDOT: PSS/SWCNT coated jute-fiber based SCs exhibit a capacitance of 17 mF cm^{-1} at 1 mV s^{-1}. The GCD analysis shows the energy and power densities of the SC are 0.712 μWh cm^{-1} and 3.85 μW cm^{-1}, respectively at a capacitance of 8.65 mF cm^{-1} for an applied current of 0.1 mA. The long charging–discharging analysis (5000 cycles) shows that the SC could work up to 13 days with a capacitive retention of 60%. By using cellulose-based materials (substrate, separator, and electrolyte) with biocompatible electrodes the presented SC offers an attractive route for sustainable energy storage and demonstrates the potential use by powering sensors suitable for applications such as smart packaging for food quality monitoring. In this regard, the developed jute/PEDOT: PSS based humidity and temperature sensors are also presented in this paper. The fabricated temperature sensor shows a relative change in response of 0.23% $°C^{-1}$ from 24 to 35 °C and the humidity sensor exhibits a sensitivity of 1.5 Ω/%RH (relative change of 0.20%) up to 50%RH. The temperature sensor was powered using the fabricated SC after the latter was charged with solar cells. The charging–discharging performance shows the potential use of the complete system in applications such as wearables, food quality, and environmental monitoring.

4. Experimental Section

Materials: In this work, PEDOT: PSS (Ossila PH 1000) and SWCNT (Sigma Aldrich) were used for electrode fabrication. EG (Acros Organic) was used for enhancing the conductivity of PEDOT: PSS. The jute fibers (length 10 cm, diameter nearly 2 mm) were purchased from the local shop. The jute fibers were sonicated for 30 min in acetone and 30 min in deionized (DI) water to remove any impurities. They were subsequently dried in the oven for 30 min at 80 °C. Ag conductive epoxy (from RS components, 186–3600) and polyester/cellulose blend separator (Techni Cloth, TX 612) were used for electrode connection and separator. Here the new electrolyte was prepared using hydroxy ethyl cellulose (Sigma Aldrich) and potassium chloride, KCl (Sigma Aldrich).

Fabrication of Fiber-Based Electrodes and SC: To coat the jute fiber, a 1:1 solution containing PEDOT: PSS (Ossila PH 1000) and EG (Acros Organic) was mixed via sonicating for 3 h at room temperature. The EG doping was used to enhance the conductivity of PEDOT: PSS by elongating the polymer backbone and facilitating the charge carrier hopping between the conducting and the insulating chains.[1,2] Here two types of electrodes were prepared to compare the performances of the jute-PEDOT: PSS based SC and the jute-PEDOT: PSS/SWCNT based SC.

i) Jute-PEDOT: PSS electrode: For this, the dried jute fibres were dipped into the PEDOT: PSS solution and left to soak for 45 min. After coating, the fibres were dried in the oven at 70 °C for 1 h. The process was repeated two times to form a uniform coating and distribution along the fibres.
ii) Jute-PEDOT: PSS/SWCNT electrode: The PEDOT: PSS coated jute fibres from step (i) were dipped in SWCNT ink for 30 min and then dried in the oven at 70 °C for 1 h.

After coating the materials on the jute fiber, an Ag conductive epoxy was painted at the end of the electrodes for external wire connection. The Ag epoxy was dried at 70 °C for 1 h in the oven and then epoxy polyurethane was coated on the top of Ag epoxy as insulation. For drying the polyurethane, the fibers were further heated in the oven at 70 °C for 3 h. The images of the prepared fiber electrodes and SC are shown in Figure S6a,b, Supporting Information. The conductive nature of the PEDOT: PSS with EG ink coated jute fiber was demonstrated by connecting it to a light-emitting diode, as shown in Figure S7, Supporting Information.

For SC fabrication, the gel electrolyte was prepared by dissolving 5 wt% of HEC in 1 M aqueous KCl salt solution in DI water at 50 °C for 3 h. The prepared gel electrolyte was coated on the top of the fiber electrode and stacked for the SC fabrication using a polyester/cellulose blend separator (Techni Cloth, TX 612) as an ion-permeable separator membrane. Figure 1a,b illustrates the cross-section of the SC and the electrode. Finally, for evaluation purpose, the SCs were packed and encapsulated in a polymer cling film and cellulose cloth (Figure 1c).

Characterization: The morphology of the jute, jute–PEDOT: PSS, and jute–PEDOT: PSS/SWCNT were observed from SEM (SU8240, BRUKER at 15 kV and WD of 8 mm) imaging. Absorption spectra were measured using a dry-air purged Bruker Vertex 70 spectrometer equipped with a globar lamp, a DLaTGS detector, and a KBr beamsplitter. 32 scans were taken at room temperature between 400 and 4000 cm^{-1} with a 4 cm^{-1} resolution. The transmission spectrum of hydroxyl-ethyl cellulose + KCl was measured with the sample placed on a microscope slide. The rest of the spectra were measured using a diamond ATR accessory (Bruker Platinum ATR Unit A225) and placing the sample directly on the diamond crystal. The electrochemical performances of the SCs were evaluated by CV, EIS, and GCD methods in a two-electrode electrochemical cell system connected to the Metrohm Autolab (PGSTAT302N, Netherland) workstation (shown in Figure S6b, Supporting Information). CV analysis was carried out at a scan rate of 1 to 100 mV s^{-1} in a potential range of 0 to 0.8 V. The EIS measurements were carried out from 1 mHz to 100 kHz at sinusoidal signals of 10 mV. The GCD measurements of the SCs were tested by using source meter (Agilent, U2722A) controlled with a LabVIEW program at a potential window 0.8 V for different applied

currents. The performance of SCs at different bending states was analyzed by static bending with a radius of 1 and 3 cm. The variation of electrical properties (resistance and capacitance) at the AC signal of 1 kHz under dynamic cyclic bending (300 cycles) were also observed. The electrochemical performance was also investigated for PEDOT: PSS–jute fiber SC tested using PVA–KCl gel electrolyte by wrapping in a beaker. The PEDOT: PSS coated jute fiber also shows repeatability in performances, as confirmed by similar response of the new devices. The electrolyte–electrode interaction for two measurements was provided through impedance data given in supporting information in Figure S8, Supporting Information. The jute fiber SC was directly charged with an amorphous silicon (a-Si) flexible solar cell (Sanyo, AT7665A 664–6841) placed under a lamp. The stored charge was discharged using a multimeter and monitored through a LabVIEW program.

Sensors Fabrication and Characterization: For humidity and temperature sensor fabrication, PEDOT: PSS coated jute fibers were prepared in a manner similar to the SC electrode fabrication. After coating the PEDOT: PSS based ink on jute fibers, their two ends were painted with Ag epoxy for external connection. The Ag epoxy coated area was insulated using polyurethane and dried at 70 °C for 1 h. For humidity studies, the sensor was placed inside a sealed gas chamber and kept at room temperature (22 °C). First, the humidity was increased to a RH of nearly 100% using a water vapor humidifier. The RH was decreased by purging nitrogen gas inside the chamber at a constant rate, varying the humidity from 95 to 17% RH. The RH and temperature were monitored by a standard digital hygrometer and temperature meter. The resistance over time was recorded using an Agilent 34465A multimeter and monitored through a LabView program. The average plateau resistance was then used to correlate the average resistance of the sensor with the RH. For temperature sensor measurement, the PEDOT: PSS coated jute fiber was packed using a cling film to reduce atmosphere influence. The fabricated sensor was inserted in a beaker and water was poured. The temperature of the water was varied using a hot plate and the temperature value was cross-checked with a thermometer. The variation of the resistance with the change in temperature was monitored using an Agilent multimeter connected to a laptop through a LabVIEW program. Repeatability measurements of the temperature sensors were also tested and provided in Figure S9, Supporting Information. Finally, for the energy-autonomous application, the flexible solar cell, fiber-based SC, and temperature sensor were attached on a jute bag.

Supporting Information

Supporting Information is available from the Wiley Online Library or from the author.

Acknowledgements

This work was supported in part by Engineering and Physical Sciences Research Council (EPSRC) through Engineering Fellowship for Growth–neuPRINTSKIN (EP/R029644/1), Royal Academy of Engineering through PHL-SENSE project (FoESFt5\100025), Royal Society-SERB Newton International Fellowship (NIF\R1\182437), IEEE Electron Device Society through new initiative project on Circular Electronics, and European Commission through AQUASENSE project (H2020-MSCA-ITN-2018-813680). M.G.J. gratefully acknowledges support through EPSRC (EP/N007417/1) and Leverhulme (RPG-2018-350).

Conflict of Interest

The authors declare no conflict of interest.

Data Availability Statement

Research data are not shared.

Keywords

cellulose, energy autonomous systems, fibre-based sensors, jute fibers, supercapacitors, sustainable energy storage, wearable electronics

Received: December 13, 2020
Revised: January 6, 2021
Published online: January 27, 2021

[1] B. Kennedy, D. Patterson, S. Camilleri, *J. Power Sources* **2000**, *90*, 156.
[2] a) H. Yim, S.-H. Yu, S. H. Baek, Y.-E. Sung, J.-W. Choi, *J. Power Sources* **2020**, *455*, 227978; b) C. García Núñez, L. Manjakkal, R. Dahiya, *npj Flexible Electron.* **2019**, *3*, 1; c) W. Gao, S. Emaminejad, H. Y. Y. Nyein, S. Challa, K. Chen, A. Peck, H. M. Fahad, H. Ota, H. Shiraki, D. Kiriya, D.-H. Lien, G. A. Brooks, R. W. Davis, A. Javey, *Nature* **2016**, *529*, 509.
[3] R. Dahiya, N. Yogeswaran, F. Liu, L. Manjakkal, E. Burdet, V. Hayward, H. Jörntell, *Proc. IEEE* **2019**, *107*, 2016.
[4] a) L. Lu, X. Han, J. Li, J. Hua, M. Ouyang, *J. Power Sources* **2013**, *226*, 272; b) G. Karimi, X. Li, *Int. J. Energy Res.* **2013**, *37*, 13.
[5] a) R. Remadevi, M. A. Al Faruque, J. Zhang, M. Naebe, *Mater. Lett.* **2020**, *264*, 127311; b) Y. K. Kim, V. Chalivendra, in *Handbook of Natural Fibres*, 2nd ed., (Eds: R. Kozlowski, M. Mackiewicz-Talarczyk), Elsevier, New York **2020**, p. 469.
[6] F. S. da Luz, M. T. G. del-Río, L. F. C. Nascimento, W. A. Pinheiro, S. N. Monteiro, *Polymers* **2020**, *12*, 1601.
[7] a) Q. Zhou, W. Teng, Y. Jin, L. Sun, P. Hu, H. Li, L. Wang, J. Wang, *Electrochim. Acta* **2020**, *334*, 135530; b) Y. Fu, H. Zhou, Z. Hu, S. Yin, L. Zhou, *Compos. Commun.* **2020**, *22*, 100446; c) J. Shi, S. Wang, Q. Wang, X. Chen, X. Du, M. Wang, Y. Zhao, C. Dong, L. Ruan, W. Zeng, *J. Power Sources* **2020**, *446*, 227345; d) M. Sun, Z. Wang, J. Ni, L. Li, *Adv. Funct. Mater.* **2020**, *30*, 1910043; e) T. Khudiyev, J. T. Lee, J. R. Cox, E. Argentieri, G. Loke, R. Yuan, G. H. Noel, R. Tatara, Y. Yu, F. Logan, *Adv. Mater.* **2020**, *32*, 2004971; f) M. Ramu, J. R. Chellan, N. Goli, P. Joaquim, V. Cristobal, B. C. Kim, *Adv. Funct. Mater.* **2020**, *30*, 1906586.
[8] L. Manjakkal, A. Pullanchiyodan, N. Yogeswaran, E. S. Hosseini, R. Dahiya, *Adv. Mater.* **2020**, *32*, 1907254.
[9] a) S. K. Gupta, S. Gupta, A. K. Gupta, *Adv. Sci., Eng. Med.* **2020**, *12*, 11; b) C. Fang, D. Zhang, *Mater. Des.* **2020**, *186*, 108322; c) P. Zhang, W. Wang, Z. Kou, B. Wang, X. Zhong, *Mater. Technol.* **2020**, *36*, 1.
[10] M. Cakici, K. R. Reddy, F. Alonso-Marroquin, *Chem. Eng. J.* **2017**, *309*, 151.
[11] a) L. Manjakkal, C. G. Núñez, W. Dang, R. Dahiya, *Nano Energy* **2018**, *51*, 604; b) R. A. Sheldon, M. Norton, *Green Chem.* **2020**, *22*, 6310; c) A. B. Lopes de Sousa Jabbour, C. J. C. Jabbour, M. Godinho Filho, D. Roubaud, *Ann. Oper. Res.* **2018**, *270*, 273; d) J. Yang, W. Cheng, K. Kalantar-zadeh, *Proc. IEEE* **2019**, *107*, 2168.
[12] L. Manjakkal, W. T. Navaraj, C. G. Núñez, R. Dahiya, *Adv. Sci.* **2019**, *6*, 1802251.
[13] a) A. Kausar, *Mater. Res. Innovations* **2020**, *25*, 53; b) M. J. Islam, M. J. Rahman, T. Mieno, *Adv. Compos. Hybrid Mater.* **2020**, *3*, 285.
[14] C. Zequine, C. K. Ranaweera, Z. Wang, P. R. Dvornic, P. K. Kahol, S. Singh, P. Tripathi, O. N. Srivastava, S. Singh, B. K. Gupta, G. Gupta, R. K. Gupta, *Sci. Rep.* **2017**, *7*, 1174.
[15] L. Mohammed, M. N. Ansari, G. Pua, M. Jawaid, M. S. Islam, *Int. J. Polym. Sci.* **2015**, *2015*, 243947.
[16] M. S. Aly-Hassan, in *Multifunctionality of Polymer Composites*, (Eds: K. Friedrich, U. Breuer), William Andrew Publishing, Oxford **2015**, p. 42.
[17] a) A. Aziz, S. S. Shah, A. Kashem, *Chem. Rec.* **2020**, *20*, 1074. b) D. P. Ferreira, A. Ferreira, R. Fangueiro, *Polymers* **2018**, *10*, 63.

[18] a) A. Lakshmanan, S. Chakraborty, *Cellulose* **2017**, *24*, 1563 b) X. Cao, B. Ding, J. Yu, S. S. Al-Deyab, *Carbohydr. Polym.* **2013**, *92*, 571; c) R.-C. Zhuang, T. T. L. Doan, J.-W. Liu, J. Zhang, S.-L. Gao, E. Mäder, *Carbon* **2011**, *49*, 2683.
[19] A. Pullanchiyodan, L. Manjakkal, S. Dervin, D. Shakthivel, R. Dahiya, *Adv. Mater. Technol.* **2020**, *5*, 1901107.
[20] M. M. Pérez-Madrigal, M. G. Edo, C. Alemán, *Green Chem.* **2016**, *18*, 5930.
[21] G. Wang, X. Lu, Y. Ling, T. Zhai, H. Wang, Y. Tong, Y. Li, *ACS Nano* **2012**, *6*, 10296.
[22] X. Ma, X. Zuo, J. Wu, X. Deng, X. Xiao, J. Liu, J. Nan, *J. Mater. Chem. A* **2018**, *6*, 1496.
[23] S. T. Senthilkumar, Y. Wang, H. Huang, *J. Mater. Chem. A* **2015**, *3*, 20863.
[24] D. Zhao, Q. Zhang, W. Chen, X. Yi, S. Liu, Q. Wang, Y. Liu, J. Li, X. Li, H. Yu, *ACS Appl. Mater. Interfaces* **2017**, *9*, 13213.
[25] a) E. P. Mwanga, E. G. Minja, E. Mrimi, M. G. Jiménez, J. K. Swai, S. Abbasi, H. S. Ngowo, D. J. Siria, S. Mapua, C. Stica, M. F. Maia, A. Olotu, M. T. Sikulu-Lord, F. Baldini, H. M. Ferguson, K. Wynne, P. Selvaraj, S. A. Babayan, F. O. Okumu, *Malar. J.* **2019**, *18*, 341; b) C. Rassie, R. A. Olowu, T. T. Waryo, L. Wilson, A. Williams, P. G. Baker, E. I. Iwuoha, *Int. J. Electrochem. Sci.* **2011**, *6*, 1949.
[26] J. Li, J.-C. Liu, C.-J. Gao, *J. Polym. Res.* **2010**, *17*, 713.
[27] V. T. Le, H. Kim, A. Ghosh, J. Kim, J. Chang, Q. A. Vu, D. T. Pham, J.-H. Lee, S.-W. Kim, Y. H. Lee, *ACS Nano* **2013**, *7*, 5940.
[28] a) Q. Chen, Y. Meng, C. Hu, Y. Zhao, H. Shao, N. Chen, L. Qu, *J. Power Sources* **2014**, *247*, 32; b) X. Zhao, B. Zheng, T. Huang, C. Gao, *Nanoscale* **2015**, *7*, 9399; c) C. Choi, S. H. Kim, H. J. Sim, J. A. Lee, A. Y. Choi, Y. T. Kim, X. Lepró, G. M. Spinks, R. H. Baughman, S. J. Kim, *Sci. Rep.* **2015**, *5*, 9387.
[29] A. Rafique, A. Massa, M. Fontana, S. Bianco, A. Chiodoni, C. F. Pirri, S. Hernández, A. Lamberti, *ACS Appl. Mater. Interfaces* **2017**, *9*, 28386.
[30] J. Ren, W. Bai, G. Guan, Y. Zhang, H. Peng, *Adv. Mater.* **2013**, *25*, 5965.
[31] F. J. Romero, A. Rivadeneyra, M. Becherer, D. P. Morales, N. Rodríguez, *Micromachines* **2020**, *11*, 148.
[32] W. A. Daoud, J. H. Xin, Y. S. Szeto, *Sens. Actuators, B* **2005**, *109*, 329.
[33] M. Kuş, S. Okur, *Sens. Actuators, B* **2009**, *143*, 177.
[34] L. Bießmann, L. P. Kreuzer, T. Widmann, N. Hohn, J.-F. Moulin, P. Müller-Buschbaum, *ACS Appl. Mater. Interfaces* **2018**, *10*, 9865.
[35] J. Zhou, D. H. Anjum, L. Chen, X. Xu, I. A. Ventura, L. Jiang, G. Lubineau, *J. Mater. Chem. C* **2014**, *2*, 9903.
[36] J.-W. Lee, D.-C. Han, H.-J. Shin, S.-H. Yeom, B.-K. Ju, W. Lee, *Sensor* **2018**, *18*, 2996.
[37] C. Bali, A. Brandlmaier, A. Ganster, O. Raab, J. Zapf, A. Hübler, *Mater. Today: Proc.* **2016**, *3*, 739.
[38] L. Manjakkal, M. Soni, N. Yogeswaran, R. Dahiya, presented at 2019 IEEE Int. Conf. on Flexible and Printable Sensors and Systems (FLEPS) Manchester, UK, July **2019**, https://doi.org/10.1109/FLEPS.2019.8792319.